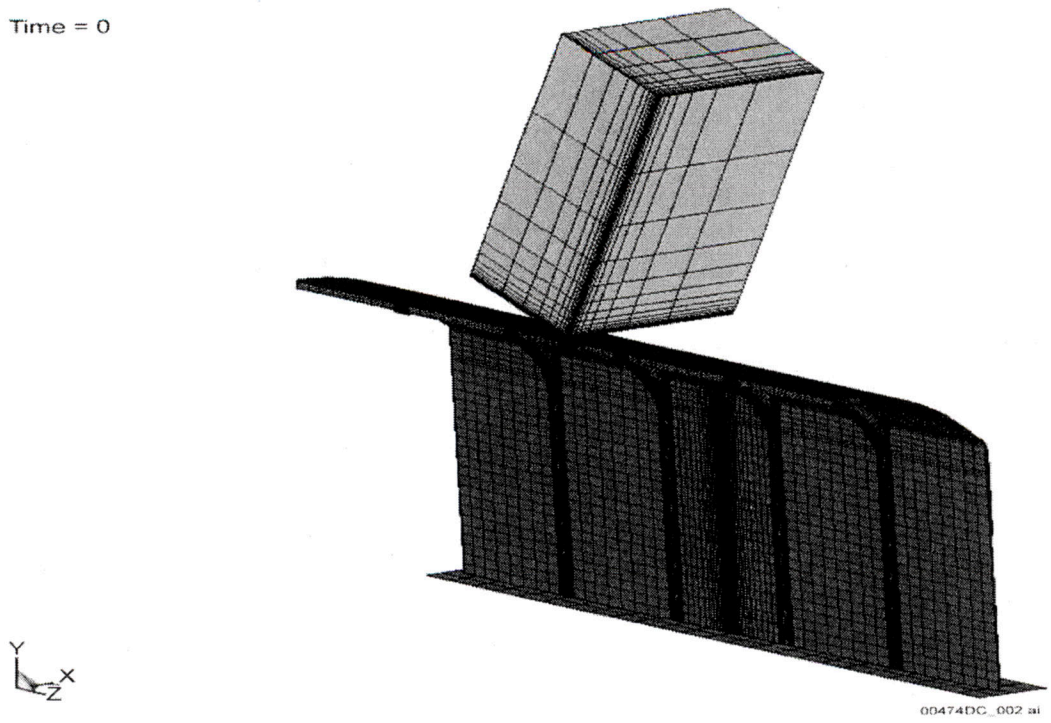

Source: Derived from BSC 2004 [DIRS 168993], Table 8-1, c1mesh4.

Figure 5-14. View of the Finite Element Representation Used for Analysis of Rock Impact

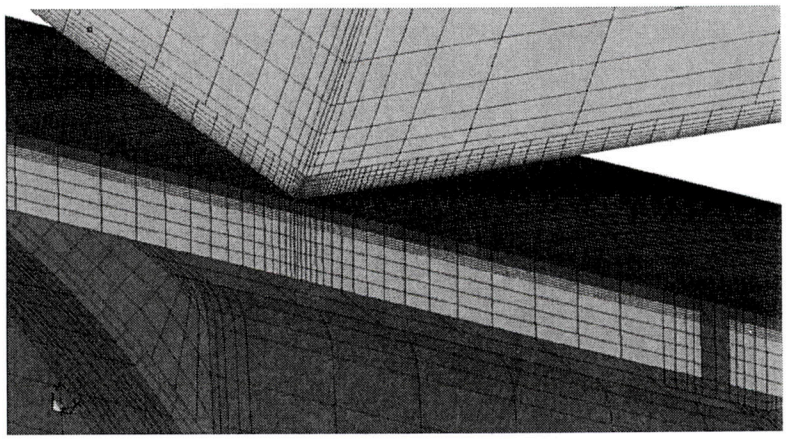

Source: Derived from BSC 2004 [DIRS 168993], Table 8-1, c1mesh4.

Figure 5-15. Detailed View of the Finite Element Representation Used for Analysis of Rock Impact

The DS corner and side-wall rockfall FE representations include an idealized waste package positioned next to the DS side-wall inside surface. The waste package is represented by rigid shells, which is used to provide a rigid boundary condition and bounding stress results for the DS.

The full-length of the DS is represented in the FE solutions. The rockfall is imposed at the mid-length of the DS, which receives no additional support from the connector plates; and hence, provides bounding stress results. Furthermore, the Alloy 22 base plate is excluded from the FE representation (Assumption 3.17). The benefit of using this assumption is to reduce the computer execution time while keeping the essential parts of the structure.

The FE representation of the impacting rock block is divided into two regions: a small, finely meshed impact region and coarsely meshed region representing the remaining part of the rock block. The continuity of deformation between these two differently meshed regions of the rock is ensured by a tied-interface contact. The fine mesh in the impact region is essential for accurate representation of the rock deformation. The elastic-ideally-plastic constitutive representation (Section 5.2.3.3) in the finely meshed region ensures realistic rock deformation and yield in the impact zone compared to the elastic rock defining the remainder of the rock block. This approach attempts to capture the localized crushing of the rock in the contact region and the consequent load distribution over the larger DS top plate area (Section 5.2.3.3).

The specified termination times of rock-fall simulation are such to allow the rock to bounce off of the DS top plate after the impact, and for steady state to establish.

The mesh of the FE representation was appropriately generated and refined in the contact regions according to standard engineering practice. Thus, the accuracy and representativeness of the results of this calculation are deemed acceptable (Section 5.2.2.4.2).

5.2.2.3 Finite Element Representation for Static Load by the Caved Rock Mass

The objective of this calculation is to investigate stability of the DS under static load of the caved rock mass, and to determine an approximate value for the factor of safety of the DS for the applied vertical and lateral static load. The three-dimensional FE representation that is used to perform the structural stability calculations is developed in TrueGrid V2.2 (Figures 5-16 through 5-18). This FE representation is limited to one segment of the DS (Figure 5-17); thus, it is referred to as the one-segment FE representation. Appropriate boundary conditions are specified at the end-sections A-A and B-B of the one-segment representation (Figure 5-17) to account for the removed part of the DS. One calculation was also performed by using the full FE representation of the DS (Figure 5-16) to verify the results obtained by using the one-segment FE representation (Section 5.4.3.2).

In the FE representations, the DS is free to move laterally with the exception of the constraint provided by the pallet (Figure 5-17) (Assumption 3.16). Note that this calculation is concerned with the quasi-static pressure induced by rock rubble. The rock rubble pressure distribution on the DS is calculated in a separate model (which couples rock mass deformation and rockfall with elastic deformation of the DS) for the DS that is in static equilibrium. The details of the modeling of emplacement drift collapse, rubblization of the rock mass and loading of the DS is presented in *Drift Degradation Analysis* (BSC 2004 [DIRS 166107], Section 6.4), and reviewed

in Section 5.2.5.1 of this document. The final deformed DS configuration, corresponding to static equilibrium under the specific rubble pressure distribution, is different from the DS configuration before the pressure application. The DS equilibrium configuration could be affected by the pallet lateral constraint depending on the pressure distribution.

All DS nodes belonging to end-sections A-A and B-B (Figure 5-12) are constrained from translating in the longitudinal (z-) direction and from rotating about the x-axis and y-axis. The following are reasons for these boundary conditions: (1) the DS (as represented in Figure 5-11) has a plane of longitudinal symmetry and its geometry for the most part consists of the repeating segments, and (2) the pressure distribution is independent of the longitudinal (z-) coordinate.

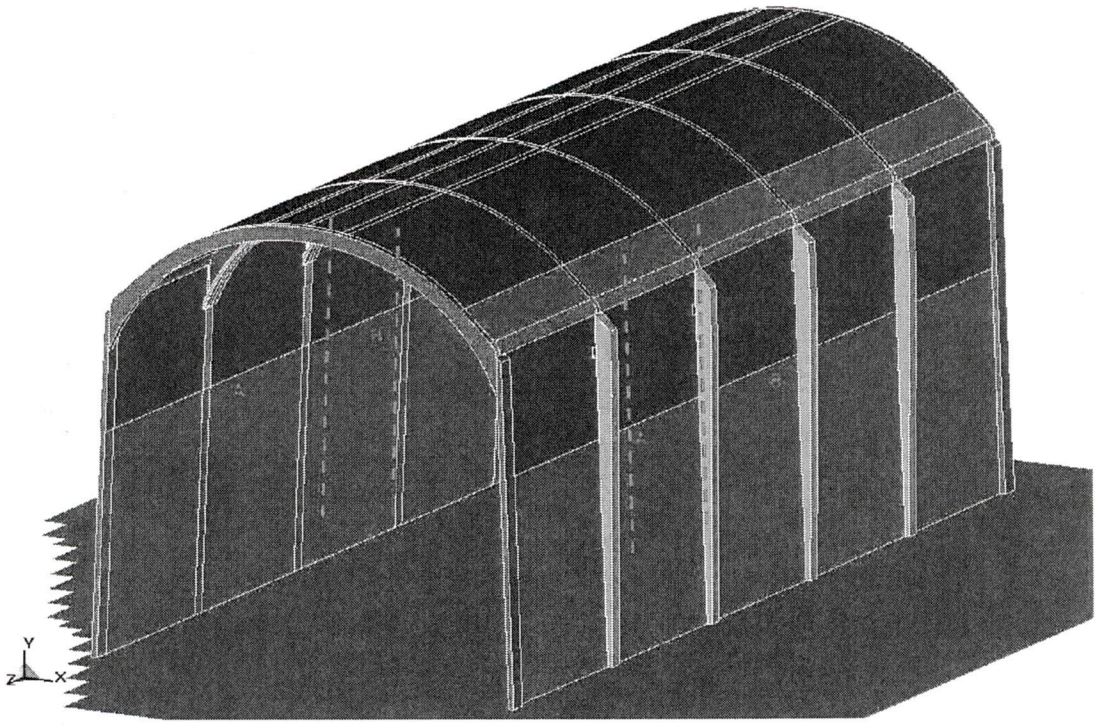

Source: BSC 2004 [DIRS 170791], Figure 1.

Figure 5-16. Full Finite Element Representation of the Drip Shield

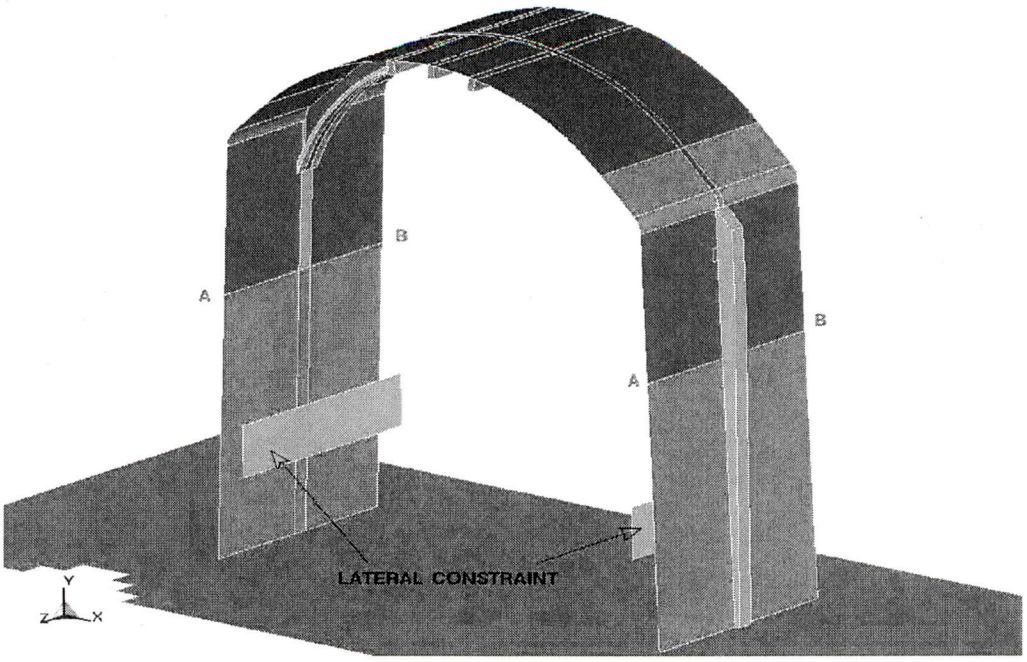

Source: BSC 2004 [DIRS 170791], Figure 2.

Figure 5-17. One-Segment Finite Element Representation of the Drip Shield

The FE representations are developed by using shell elements for the DS plates (specifically, DS plate-1, DS plate-2, and support plates), and solid (brick) elements for the rest of the structure (i.e., the support beams, bulkheads, bulkhead longitudinal stiffeners, etc.; see BSC 2004 [DIRS 170791], Attachment I). The details of the FE representation are illustrated in Figure 5-18. The fully-integrated four-node shell element (Livermore Software Technology Corporation 2003 [DIRS 166841], p. 26.22) and the constant-stress eight-node solid element (Livermore Software Technology Corporation 2003 [DIRS 166841], p. 26.30) are used for all calculations. Gauss integration and five through-thickness integration points (Livermore Software Technology Corporation 2003 [DIRS 166841], p. 26.23) are specified for the shell element. One-point Gaussian quadrature is used for the solid element (Hallquist 1998 [DIRS 155373], Section 3).

5.2.2.4 Mesh Objectivity

The objectivity (mesh insensitivity of the calculations) of the meshes used for the calculations is verified in this section. The approach used is presented in detail in Mecham (2004 [DIRS 170673], Section 6.2.3). Two different meshes of the DS are generated and used in the FE simulation. The first mesh is obtained by following the standard engineering practice and guidance in Mecham (2004 [DIRS 170673], Section 6.2.3). The second mesh is a refined version of the first mesh. The results obtained by the first mesh are considered mesh-objective (i.e., mesh-insensitive) if the relative difference of results (e.g., damaged area) between the first and the second mesh are much smaller (approximately an order of magnitude smaller) than the relative difference of areas (or volumes) of their representative (average, typical) elements.

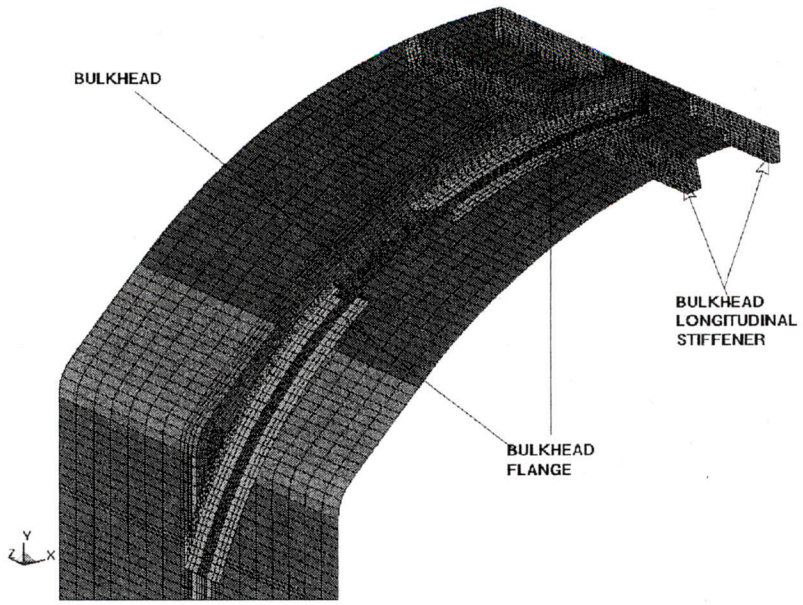

(a)

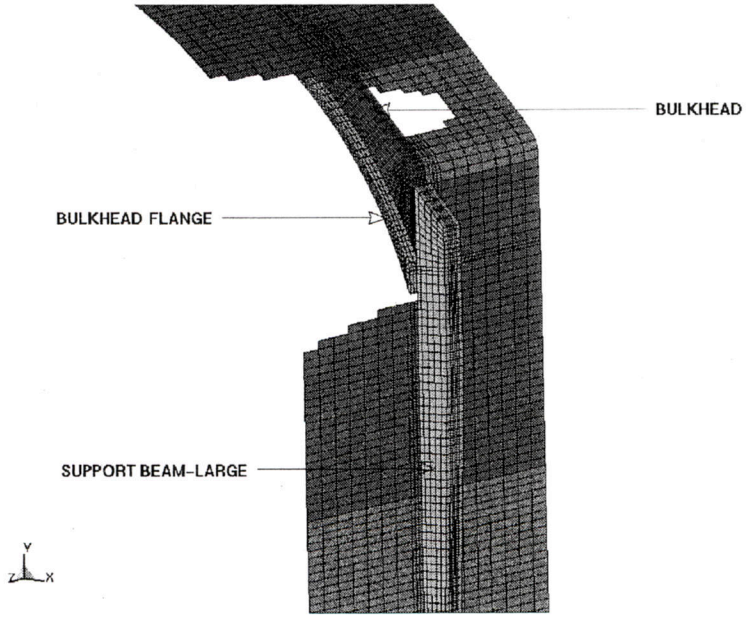

(b)

Source: BSC 2004 [DIRS 170791], Figure 3.

NOTE: Some DS parts are partially removed from Figure 5-13 to improve visibility; (a) top (inside view) and (b) side (outside view).

Figure 5-18. Details of Finite Element Representation of the Drip Shield

5.2.2.4.1 Vibratory Ground Motion

The typical DS shell element area of the first mesh is 300 percent (four times) larger than the area of the corresponding element in the second mesh. Element number 6442 of the first mesh and element number 9617 of the second (refined) mesh can be compared as typical elements for the two FE representations.

The mesh sensitivity of the DS damaged area is studied for realization 10 (Table 5-17) at 1×10^{-6} annual frequency of occurrence. The results are presented in Table 5-1.

Table 5-1. Damaged DS Area for Two Different FE Meshes for Realization Number 10 (1×10^{-6} Annual Frequency of Occurrence)

Mesh	Damaged Area (m^2; % of DS plate area)
First Mesh $A = 4A_0$	0.192; 0.502
Second Mesh $A = A_0$	0.169; 0.441

Source: BSC 2003 [DIRS 163425], Table III-1.

According to results presented in Table 5-1 the reduction of typical element size by 300 percent for realization 10 results in decrease of the damaged area by 12.0 percent.

The decrease of the damaged area in the case of the refined mesh can be explained by more localized DS deformation (following the impacts between DS and waste package pallet assembly) for the refined mesh compared to the one for the coarser mesh. Thus, the results obtained by using the first mesh meet the mesh-objectivity criterion from Mecham (2004 [DIRS 170673], Section 6.2.3). Namely, a coarse mesh is inherently less capable of accommodating localized deformation (it is less flexible to do so). Consequently, the impact energy delivered to the DS plate is smeared over a larger area. In other words, the redistribution of the impact energy over a larger area is caused by the inherent inability of the (less flexible) coarse mesh to capture the localized deformation. In the case of a relatively low damage threshold, the results of fine mesh calculations leads to overestimation of the damaged area by the coarse mesh model. The stress averaging within a relatively coarse constant-stress element is, consequently, likely to overestimate the damaged area.

5.2.2.4.2 Rock Impact in Nonlithophysal Rock Mass

The values of two stress invariants (stress intensity and the maximum first principal stress) are presented for two different meshes in Table 5-2. The DS top plate element volume at the point of impact in the first mesh is 67 percent larger than the corresponding element in the second mesh ($5.148\times10^{-8}/3.089\times10^{-8} = 1.67$). Specifically, the numbers of divisions in the axial, tangential, and thickness directions are increased from 14 to 16, from 4 to 5, and from 5 to 6, respectively. The calculation results presented in Table 5-2 indicate that the reduction of the element volume by 67 percent in the contact region results in negligible effect on the stress intensity. The difference in the first principal stress values between the two meshes is a little bit

more pronounced, but still meets the mesh-objectivity requirements in Mecham (2004 [DIRS 170673], Section 6.2.3). The original FE mesh is, therefore, deemed acceptable and all remaining calculations are performed with the coarser mesh.

Table 5-2. Stress Intensity and First Principal Stress for Two Different FE-Representation Meshes (14.5 MT Vertical Rockfall)

	Stress Intensity (MPa)	First Principal Stress (MPa)
First Mesh V = 1.67 Vo	346	340
Second Mesh V = Vo	352	363
Difference (%)	1.7	6.3

Source: BSC 2004 [DIRS 168993], Table 6-1.
MT: metric tons (1 MT = 1000 kg)

5.2.2.4.3 Static Load by the Caved Rock Mass

The volumes of the typical elements for the support beam and bulkhead for two different meshes are presented in Table 5-3. The numbers presented in Table 5-3 in parentheses represent the number of the element that is considered typical.

As described in Section 5.2.5.1, the rock rubble loads derived from 6 realizations of drift collapse provided in *Drift Degradation Analysis* (BSC 2004 [DIRS 166107], Section 6.4.2.5), are applied to the outer surface of the DS to investigate structural stability and damage. As a part of this study, the ultimate load-bearing capacity of the DS is examined by artificially increasing the density of the rubble to force increasing loads until failure of the DS occurs. The rubble density was increased in a number of steps from 1 to 4 times, with 6 realizations conducted at each density step. The mesh sensitivity was studied in particular for the case in which the average loads from all 6 realizations with a density multiplication factor of 2.5 was used (discussed in Section 5.4.3.1). The choice of this realization is arbitrary: the mesh-objectivity results should not depend on the particular pressure distribution. The calculation with the density of the surrounding rock multiplied by 2.5 is interesting because it illustrates an approximate stability safety margin for the DS for that pressure distribution (Section 5.4.3.2). The results are presented in Table 5-4.

According to results presented in Tables 5-3 and 5-4, the calculation results are not mesh-sensitive.

Table 5-3. Volume of Typical Element for Two Different Finite Element Meshes

DS Component	Volume of Typical Element ($1 \cdot 10^{-6}$ m^3)		
	First Mesh	Second Mesh	Relative Difference (%)
Bulkhead	1.38 (e# 6453)	0.85 (e# 15798)	62
Support Beam	2.47 (e# 4800)	1.46 (e# 12614)	69
	5.21 (e# 4888)	1.92 (e# 12854)	171

Source: BSC 2004 [DIRS 170791], Table V-1.

Table 5-4. Maximum Vertical Displacement of Drip Shield Top for Two Different Finite Element Meshes

Maximum Vertical Displacement ($1 \cdot 10^{-3}$ m)		
First Mesh	Second Mesh	Relative Difference (%)
19.08	18.92	0.8

Source: BSC 2004 [DIRS 170791], Table V-2.

5.2.2 Material Properties

Material properties used in these calculations are discussed in this section. The basic material properties required as input to these analyses include the mechanical properties of Ti-7 and Ti-24, as well as the mechanical properties of the rock blocks (termed TSw2). The DS temperature is assumed to be 150°C (Assumption 3.12). Some of the temperature-dependent and rate-dependent material properties are not available for Ti-7, Ti-24 and TSw2 rock. Therefore, RT Poisson's ratio, elongation, and modulus of elasticity obtained under the static loading conditions are used for these materials (Assumptions 3.1 through 3.3).

5.2.3.1 Titanium

Typical stress-strain curves for Ti-7, Ti-24 and Alloy 22, and their idealizations used in numerical analyses are shown in Figure 5-19. Material properties of Ti-7 (SB-265 R52400) are given in Table 5-5.

Material properties of Ti-24 (SB-265 R56405) are similar to those of Ti-5 because the compositions are almost identical (ASME 2001 [DIRS 158115]), Section II, Part B, SB-265, Table 2). These material properties, given in Table 5-6, are specified using the nominal composition, 6Al-4V.

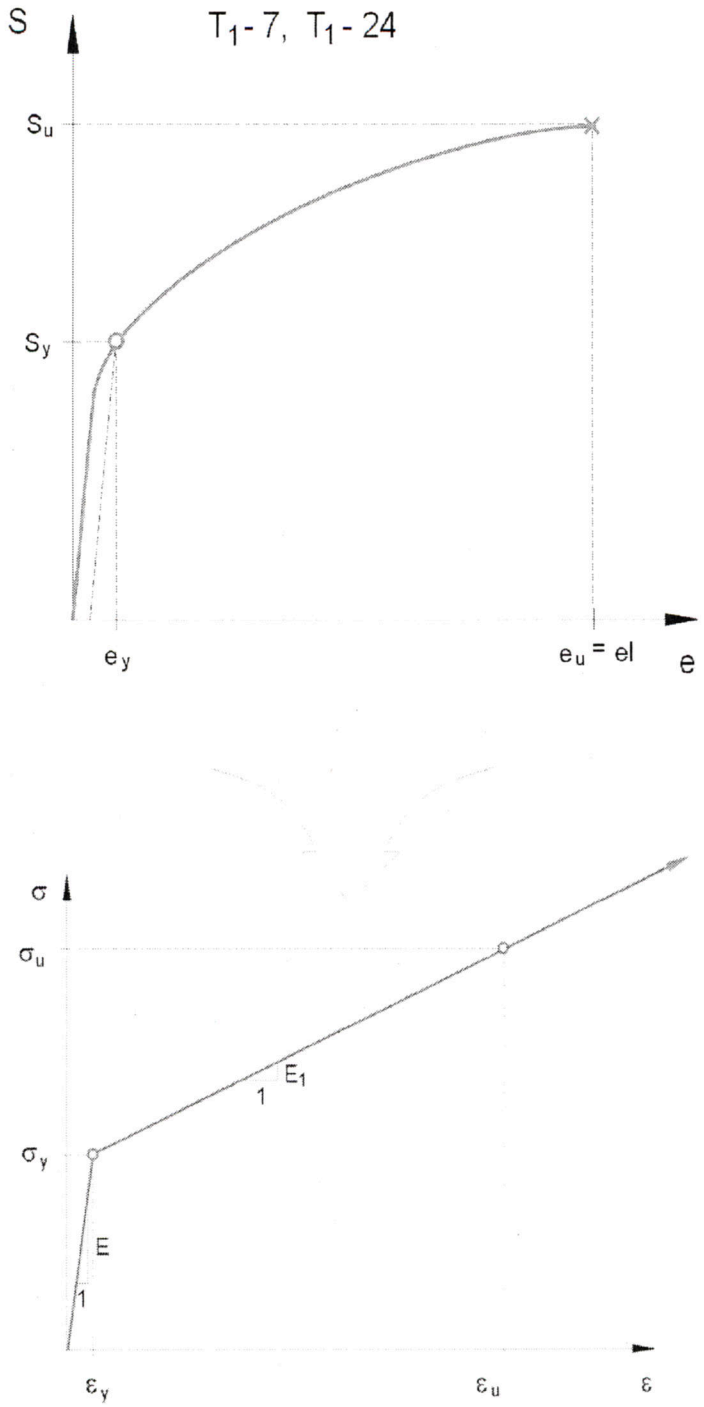

Figure 5-19. Typical and Idealized Stress-Strain Curves for Titanium Grades 7 and 24

Table 5-5. Material Properties of Ti-7 (SB-265 R52400)

Property	Temperature [°C]/[°F]	Range	Value	Source
Young's Modulus E [GPa]	149/300	—	101	MO0003RIB00073.000 [DIRS 152926], page 3
	204/400	—	97	MO0003RIB00073.000 [DIRS 152926], page 3
Density ρ [kg/m^3]*	RT	4500-4540	4520	MO0003RIB00073.000 [DIRS 152926], page 1
Poisson's Ratio ν	RT	—	0.32	MO0003RIB00073.000 [DIRS 152926], page 3
Yield Strength s_y [MPa]*	RT	275-450	363	MO0003RIB00073.000 [DIRS 152926], page 2
	204/400	138-152	145	MO0003RIB00073.000 [DIRS 152926], page 2
Tensile Strength s_u [MPa]*	RT	—	345	MO0003RIB00073.000 [DIRS 152926], page 2
	204/400	207-228	218	MO0003RIB00073.000 [DIRS 152926], page 2
Elongation e_u	RT	—	0.2	MO0003RIB00073.000 [DIRS 152926], page 2
	204/400	0.38-0.45	0.42	MO0003RIB00073.000 [DIRS 152926], page 2

NOTE: An average value is used in the calculations described in this document, as the number of data points available does not justify the assumption of a distribution of values.

*Values rounded to nearest whole number.

RT = room temperature

Table 5-6. Material Properties of Ti-24 (SB-265 R56405)

Property	Temperature [°C]/[°F]	Range	Value	Source
Young's Modulus E [GPa]*	RT	107-122	115	TIMET 2000 [DIRS 160688], table 2
	230/450	95-111	103	TIMET 2000 [DIRS 160688], table 2
Density ρ [kg/m^3]*	RT	—	4430	ASM 1990 [DIRS 141615], page 620
Poisson's Ratio ν	RT	—	0.34	ASM 1990 [DIRS 141615], page 621
Yield Strength s_y [MPa]*	RT	—	910	TIMET 1993 [DIRS 157726], page 11
	204/400	—	683	TIMET 1993 [DIRS 157726], page 11
Tensile Strength s_u [MPa]*	RT	—	1000	TIMET 1993 [DIRS 157726], page 11
	204/400	—	772	TIMET 1993 [DIRS 157726], page 11
Elongation e_u	RT	—	0.18	TIMET 1993 [DIRS 157726], page 11
	204/400	—	0.17	TIMET 1993 [DIRS 157726], page 11

NOTE: An average value is used in the calculations described in this document, as the number of data points available does not justify the assumption of a distribution of values.

*Values rounded to nearest whole number.

RT = room temperature

5.2.3.1.1 Calculation for Material Properties at Elevated Temperature

Some of the material properties of Ti-7 and Ti-24 are not available at $T_{max} = 150\,^{o}C$ (Section 5.2.3.1). They are, therefore, obtained (Table 5-7) by linear interpolation using the following relation:

$$P = P(T) = P_l + \left(\frac{T - T_l}{T_u - T_l}\right) \cdot (P_u - P_l), \qquad \text{(Eq. 5-6)}$$

where subscripts u and l denote the bounding values of the property (P) at the corresponding bounding temperatures (T).